Journal of The Electrochemical Society, **159** (2) H102-H106 (2012)
0013-4651/2012/159(2)/H102/5/$28.00 © The Electrochemical Society

High-Purity Ultraviolet Electroluminescence from *n*-ZnO Nanowires/p^+-Si Heterostructure LEDs with *i*-MgO Film as Carrier Control Layer

Byung Oh Jung,[a] Ju Ho Lee,[b] Jeong Yong Lee,[b] Jae Hyun Kim,[c,z] and Hyung Koun Cho[a,z]

[a] *School of Advanced Materials Science and Engineering, SungKyunKwan University, Suwon 440-746, Korea*
[b] *Department of Materials Science and Engineering, KAIST, Daejeon 305-701, Korea*
[c] *Department of Nano and Bio Technology, DGIST, Daegu 704-230, Korea*

Pure ultraviolet (UV) light emitting diodes (LEDs) using *n*-ZnO nanowires as an active layer were fabricated with an insulating MgO dielectric layer as a carrier control layer, where all depositions were continuously performed by metalorganic chemical vapor deposition. The current-voltage curve of the LEDs showed obvious rectifying characteristics, with a threshold voltage of about 7 V in the sample with 4 nm *i*-MgO. Under the forward bias of the samples with proper MgO thickness, a sharp UV electroluminescence, located at around 380 nm, was emitted from the active ZnO nanowires, while weak visible emission of around 450–700 nm were observed. The pure UV emission from the ZnO nanowires in the *n*-ZnO/*i*-MgO/p^+-Si heterostructures was attributed to the electron accumulation in the ZnO by asymmetric band offset and preemptive hole tunneling from Si to ZnO by *i*-MgO.
 [DOI: 10.1149/2.029202jes]

Manuscript submitted September 15, 2011; revised manuscript received October 31, 2011. Published December 16, 2011.

Low-dimensional nanostructure materials have attracted great interest in various research fields due to their unique physical and chemical properties.[1] Along with various other materials, zinc oxide (ZnO) with a direct bandgap of 3.37 eV and a large exciton binding energy of 60 meV, has been widely investigated for potential optoelectronic applications, such as laser devices, optical sensors, solar cells, and light emitting diodes (LEDs).[1–4] Further, ZnO nanostructures have been considered as a candidate material for the next generation blue and near-UV light sources due to their large emissive areas. In particular, one-dimensional ZnO nanostructures including nanowires, nanobelts, nanorods, and nanowalls can be easily synthesized in large quantities on several substrates.[5–8]

In previous research, some approaches have been developed to synthesize *n*-ZnO nanostructure-based heterostructures using *p*-GaN, *p*-SiC, *p*-NiO, and *p*-AlGaN as a *p*-type material.[9–12] Among them, the *p*-GaN is the most promising due to high-quality ZnO/GaN heterojunctions induced from the same wurtzite structure and small in-plane lattice mismatch (1.8%). However, the ZnO/GaN heterojunction LEDs are economically infeasible, due to their low emission efficiency, compared to the GaN based LEDs (InGaN/GaN, AlGaN/GaN, etc.). On the other hand, the heterojunction LEDs using *p*-Si substrates are cost effective and utilize well-developed fabrication processes. The ZnO/Si heterostructure has asymmetrically large band offset between two energy bandgaps, since the ZnO has wider bandgap energy (3.37 eV) than Si (1.12 eV). Interestingly, asymmetric band offset can provide an effective hole carrier injection from *p*-Si to ZnO, by blocking the flow of electrons in the ZnO/Si interface. Thus, the fabrication of the LEDs using the ZnO nanowires and thin films deposited on the Si substrates has been studied for the fabrication of UV LEDs. However, the *n*-ZnO/*p*-Si heterostructures cause high leakage in the current and very low emission efficiency. In particular, most *n*-ZnO/*p*-Si heterostructure LEDs showed relatively strong visible emission and weak UV emission, and thus were mainly applied as sensor devices such as optical and chemical sensors.[13] To resolve this problem, the appropriate dielectric layers with proper band offset were suggested and these layers restricted the movement of electrons or holes, resulting in the emission in the ZnO. Unfortunately, the use of the Si substrate causes degradation in the crystalline quality of the ZnO film, induced by the formation of polycrystalline. In contrast, the growth of the nanowires on the Si substrates induces the single crystal ZnO without structural defects. Therefore, the selection of the appropriate dielectric layer and the growth of the ZnO nanowires on the Si substrates is expected to provide a very promising method for the fabrication of high-purity UV LEDs.

In this study, we present the ZnO nanostructure based UV LEDs, introducing dielectric insulating layers with proper thickness and realizing the pure UV LEDs from the ZnO nanowires. We chose the insulating MgO (*i*-MgO) deposited by metalorganic chemical vapor deposition (MOCVD) as a current control layer. All synthesized products such as *n*-ZnO nanowires and *i*-MgO were fabricated by MOCVD on p^+-Si substrate. The *n*-ZnO/*i*-MgO (4 nm)/p^+-Si heterostructure LED emitted an intense UV EL spectrum (around 380 nm) coming from the ZnO nanowires. The mechanism for the EL emission, depending on the thickness of inserted *i*-MgO layers, was discussed with band offset engineering and tunneling current.

Experimental

Prior to the deposition of the vertically arrayed ZnO nanowires, the *i*-MgO layers were grown for different times on p^+-Si substrates via MOCVD technique, as reported elsewhere.[14] The *i*-MgO layers were synthesized at 550°C and 1 Torr using cyclopentadieny magnesium (Cp_2Mg) and high-purity oxygen gas reactants. High-purity argon was also used as the carrier gas for Cp_2Mg. The growth times for the *i*-MgO were 0 (sample 1), 10 (sample 2), 20 (sample 3), and 30 minutes (sample 4) to investigate the thickness effects of the *i*-MgO layers on electroluminescence (EL) and electric characteristics. The *i*-MgO layers were applied as a current control layer to block the direct electron flow from the *n*-ZnO nanowires to the p^+-Si substrate. After the growth of the MgO, the dense ZnO nanowires were continuously grown as active layers without pausing growth in the MOCVD chamber. The synthesis of the ZnO nanowires was carried out at 400°C and 1 Torr for 30 minutes using diethylzinc (DEZn) and high-purity oxygen gas. Argon was used as the carrier gas for the DEZn. The flow rate of reactive oxygen gas was set to 50 SCCM, while the argon flow rate was maintained at 10 SCCM.

Morphology observations of the *n*-ZnO nanowires on the *i*-MgO layer coated p^+-Si substrates were investigated by field-emission scanning electron microscopy (FE-SEM, JSM-7600F) operated at 10 kV. Transmission electron microscopy (TEM, JEM-3010) was used to measure the thickness of *i*-MgO layers. Figure 1a shows a schematic diagram of the *n*-ZnO/*i*-MgO/p^+-Si heterostructure LED designed in this research. Extensively, the *p*-Si/Ag and *n*-ZnO/ITO contacts show well-defined ohmic properties.[15,16] For the *n*-ZnO/ITO contacts, flexible polymer sheets coated with ITO were used to enlarge the contact yield between the *n*-ZnO nanowires and the ITO electrode. The use of soft polymer substrates results in good electrical contact on the surface of the nanowires with different lengths and forms more

[z] E-mail: jaehyun@dgist.ac.kr; chohk@skku.edu

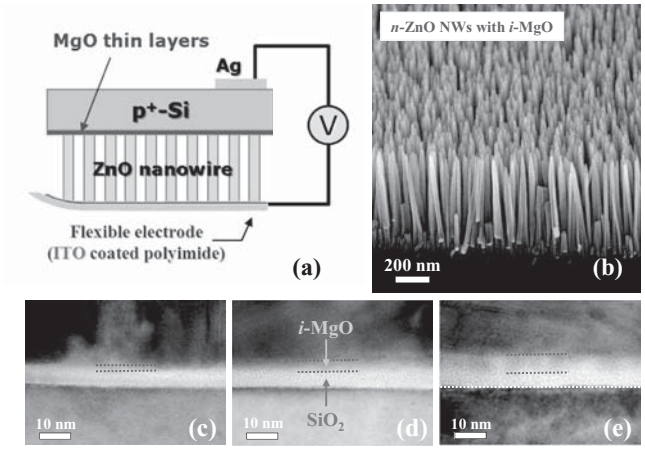

Figure 1. (a) Schematic diagram of *n*-ZnO nanowires/*i*-MgO/p^+-Si heterostructure LED used in this study. (b) Cross-sectional SEM image of ZnO nanowires on the p^+-Si substrate coated with *i*-MgO layer (6 nm) (sample 4). High magnification TEM images showing the thickness of oxide layers: (c) sample 2, (d) sample 3, and (e) sample 4.

stable contact than ITO coated glass substrates. The current-voltage (*I-V*) measurements of the grown *n*-ZnO nanowires/*i*-MgO/p^+-Si heterostructure LEDs were performed with an HP4145B semiconductor parameter analyzer. The photoluminescence (PL) measurements of the *n*-ZnO nanowires/*i*-MgO/p^+-Si heterostructures were carried out at room-temperature using a He-Cd laser operating at 325 nm. The EL measurements were also conducted under forward bias condition at room-temperature.

Results and Discussion

In the previous study, we have devised a method to grow ultrathin *i*-MgO layers with amorphous phases using MOCVD for the fabrication of the ZnO nanowire based sensors, and suggested that the ultrathin *i*-MgO can control the band offset between ZnO nanowires and Si with proper layer thickness.[14] Figure 1b shows the cross-sectional SEM image of the ZnO nanowires grown on the p^+-Si substrate coated with *i*-MgO (6 nm), where the ZnO nanowires were uniformly grown with high density and vertical array. The length and diameter of these ZnO nanowires are about 600 ~ 650 nm and 20 ~ 30 nm, respectively. Prior to the growth of the nanowires, the *i*-MgO layers were deposited with different thicknesses. The primary purpose on the introduction of the *i*-MgO layer is to control carrier flow by adjusting *i*-MgO thickness. Some research groups grew the *i*-MgO layers with a cubic phase as a carrier blocking layer before the deposition of the ZnO thin film, because the ZnO films could be epitaxially grown on the cubic MgO, expecting high-quality single-crystalline and good optical properties of the ZnO films. However, the cubic MgO layers can be grown by limited methods such as molecular beam epitaxy (MBE) and electron beam evaporation (e-beam).[17,18] In addition, the MgO layer generally has a very low growth rate and needs a thickness of over 50 nm to grow epitaxial ZnO film on the MgO layer. Unfortunately, the thicker MgO layer leads to significant reduction of the current level for both forward and reverse bias. As a result, degradation in the EL emission efficiency of the ZnO/Si heterostructure LEDs was caused, showing weak UV emission and intense deep-level emission. In contrast, MgO thin layers deposited by MOCVD didn't influence vertical arrays and crystal quality of ZnO nanowires despite their amorphous phase, and also have insulating electrical properties. Thus, it is expected that they can effectively control the carrier flow in the fabrication of ZnO nanowire based LEDs. Figures 1c–1e exhibit high magnification TEM images obtained from the *n*-ZnO/*i*-MgO/p^+-Si heterostructures with various MgO thicknesses. As shown in these figures, the thin MgO layers with dark contrast exist on p^+-Si substrate with the form of amorphous phase. The bright contrast on the p^+-Si corresponds to the native silicon oxide (SiO_2) layers. The SiO_2 thickness on the p^+-Si substrate is roughly 5 nm and the total thickness of oxide layers accords to the sum of SiO_2 and *i*-MgO layers. The total oxide thicknesses including the *i*-MgO layer on the p^+-Si substrates are approximately 7, 9, and 11 nm for samples 2, 3, and 4, respectively.

Figures 2a–2d show the *I-V* characteristics of the *n*-ZnO nanowires/p^+-Si substrate heterostructure LEDs with and without the *i*-MgO layer, measured under dark dc bias condition. Also, the insets exhibit the series resistance (R_S) of measured samples. The R_S can be obtained by calculating the slope in an *I/(dI/dV)* versus *I* graphs in the high voltage region ($V > E_{g/q}$, where E_g is energy bandgap) of the *I-V* curves.[19] According to the *p–n* junction theory, the *I–V* characteristics of real diodes can be expressed as,[4,20]

$$I = I_S \left\{ \exp\left[\frac{q\,(V - IR_S)}{nkT} \right] \right\} - 1 \qquad [1]$$

where, *k* is Boltzmann's constant, *n* is ideality factor, *T* is temperature in Kelvin, and I_S is the reverse saturation current. Figure 2a shows that *n*-ZnO/p^+-Si heterostructure without MgO doesn't exhibit well rectifying characteristic observed in the diode, which is attributed to the small conduction band offsets (CBO) of roughly 0.3 eV at the ZnO/Si interface.[21] The *n*-ZnO/p^+-Si junction has a relatively large band offset in the valence band, and thus the CBO determines the amount of the charge carrier flow. Therefore, for the *n*-ZnO/p^+-Si heterostructure, the electrons in *n*-ZnO nanowires freely move into the Si under DC bias conditions, resulting in active current flow. On the other hand, Figs. 2b–2d illustrate that the *n*-ZnO/*i*-MgO/p^+-Si heterostructures behave like a well-defined diode with rapid current increase under forward bias and blocking of the current flow under reverse bias. The forward bias turn-on voltage was about 7 V in sample 2, and was increased by increasing the *i*-MgO thickness. The higher turn-on voltages in sample 3 and sample 4 were attributed to the voltage drop across the insulating dielectric layer.[11] Additionally, as shown in the insets of Figs. 2b–2d, the typical values of the R_S were estimated to be 1.2 kΩ for sample 2, 150 kΩ for sample 3, and 180 MΩ for sample 4. The increase in R_S was also due to the high resistance properties in the thicker *i*-MgO layers, which was entirely consistent with higher threshold voltage for the samples with thicker *i*-MgO layers.

Figure 3a displays the room-temperature PL spectra of the *n*-ZnO/*i*-MgO/p^+-Si heterostructures. Samples 1 ~ 4 exhibit similar PL spectra of strong UV emission peaks positioned at about 375 nm and undistinguishable deep level emissions, indicating high crystalline and optical quality of the nanowires. The UV emission peak at room temperature mainly originated from the excitonic transition between valence and conduction bands.[22] The center position of UV emission is the same for samples 3 and 4. Figure 3b shows the EL spectra from the *n*-ZnO/*i*-MgO/p^+-Si heterostructure LEDs with different *i*-MgO thickness. The heterostructure LEDs consist of two distinguishable peaks centered at around 380 and 575 nm. By comparing the EL spectrum with the PL spectrum, it is considered that the sharp peak at 380 nm is attributed to a radiative recombination corresponding to near band edge emission from *n*-ZnO nanowires, while the peak at 575 nm comes from the defects of *n*-ZnO nanowires. We have previously reported that the broad peak at around 575 nm from the ZnO grown by MOCVD was related to excess oxygen interstitial.[22] Most studies on EL performance using ZnO films and nanowires show different emission position in the PL and EL measurements. However, our nanowires exhibit almost similar emission centers. Unlike previous reports on the synthesis of the nanowires using crystal seed layers, our nanowires were fabricated on noncrystal MgO and this leads to the formation of nearly stress free ZnO nanowires. In thin film technology, stress mainly originates from lattice mismatch at the interfaces and structural defects such as grain boundaries. It is well-known that ZnO nanowires with single crystals are preferentially grown along the polar *c*-axis, and this induces the polarization field and band bending along the growth direction, resulting in the shift of emission position and the

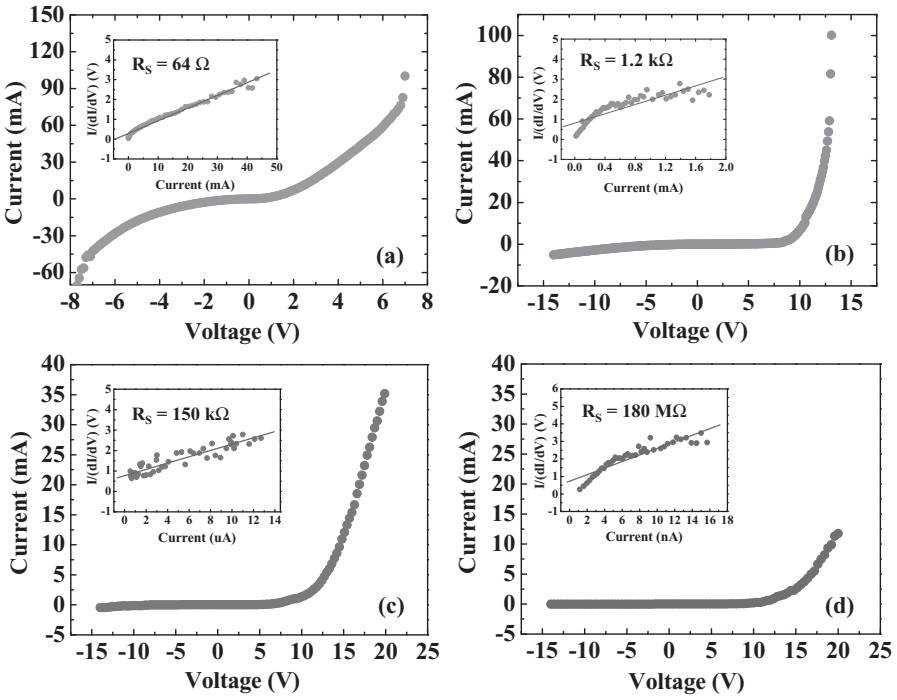

Figure 2. The current-voltage (*I-V*) characteristics of the *n*-ZnO nanowires/*i*-MgO/p^+-Si heterostructures: (a) sample 1, (b) sample 2, (c) sample 3, and (d) sample 4.

degradation of emission efficiency. Meanwhile, the *n*-ZnO nanowires on the *i*-MgO in this study show similar EL and PL peak position and strong pure UV emission due to the absence of the interfacial stress.

Figure 4 presents the band structure model to help understanding of the carrier transportation process depending on the *i*-MgO layer thickness. We considered that the electron affinities of ZnO, MgO, and Si are 4.35, 0.8, and 4.05 eV, respectively,[23–25] as shown in Fig. 4a. Upon applying forward bias to *n*-ZnO/*i*-MgO/p^+-Si LEDs, the energy band of Si would be moved more downward than that of ZnO nanowires. For the sample with thinner *i*-MgO, as shown in Fig. 4b, the carriers can migrate between ZnO and Si through tunneling due to the ultrathin *i*-MgO layer, which cannot block the flow of carriers at the interfaces of *n*-ZnO/*i*-MgO and p^+-Si/*i*-MgO. This leads to a dramatic increase in the forward current at low bias, as shown in Fig. 2b. The *i*-MgO layer of about 2 nm (sample 2) was too thin to accumulate the carriers and did not induce radiative recombination, due to the disturbance of the overlapping of electron and hole. However, it shows an increase in the threshold voltage and decrease in leakage current, as increasing the MgO thickness, where the current level at 15 V in sample 2 is one order of magnitude higher than that in sample 3.

Nevertheless, it is expected that the *i*-MgO layer with proper thickness is effective in inducing radiative recombination in the *n*-ZnO nanowire arrays. Considering electron affinity and bandgap energy, the CBO at the *n*-ZnO/*i*-MgO interface is about 3.6 eV,[26] and calculated value of the valence band offsets (VBO) on considering electron affinity and bandgap energy at the p^+-Si/*i*-MgO interface is about 2.8 eV, as marked in Fig. 4d. This indicates that the insertion of the *i*-MgO layer induces the blocking of charge carriers in the conduction band of the ZnO and the valence band of the Si.[26] As a result, the majority of carriers in *n*-ZnO nanowires (electrons) and p^+-Si (holes) would be accumulated at the interfaces of *n*-ZnO/*i*-MgO and p^+-Si/*i*-MgO, respectively, under forward bias, if the *i*-MgO layers have proper thickness. Unlike sample 2, showing tunneling in the ultrathin MgO, the *i*-MgO thickness in samples 3 and 4 do not allow electron carriers to flow actively between *n*-ZnO and p^+-Si at low bias, due to thicker MgO thickness and band offset. However, the holes at the *i*-MgO/p^+-Si interface can move to *n*-ZnO nanowires over threshold voltage, because the VBO between Si and MgO is relatively low. It leads to the radiative recombination in the *n*-ZnO nanowire side with direct band, particularly pure UV emission, as shown in Fig. 3. Additionally, the UV emission coming from the tunneling of hole carriers

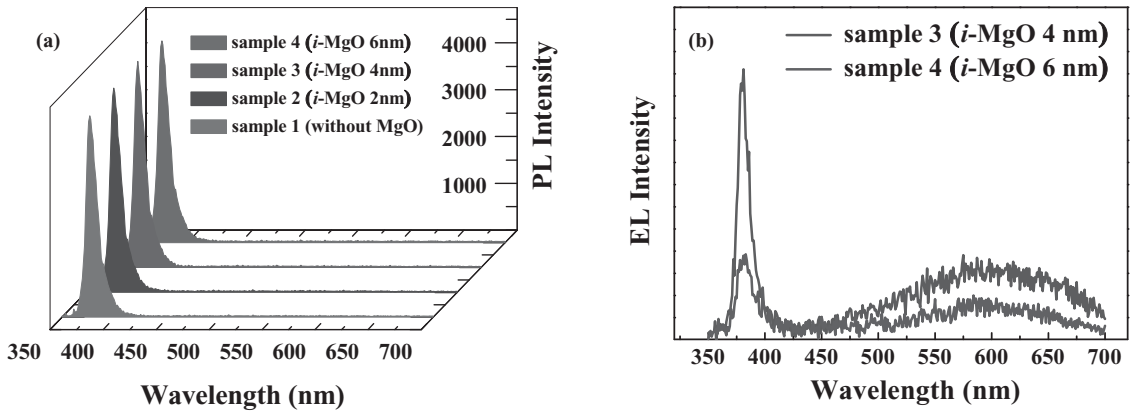

Figure 3. (a) Normalized PL spectra for samples 1, 2, 3 and 4, and (b) RT EL spectra for sample 3 and sample 4 under the applied bias of 15 V.

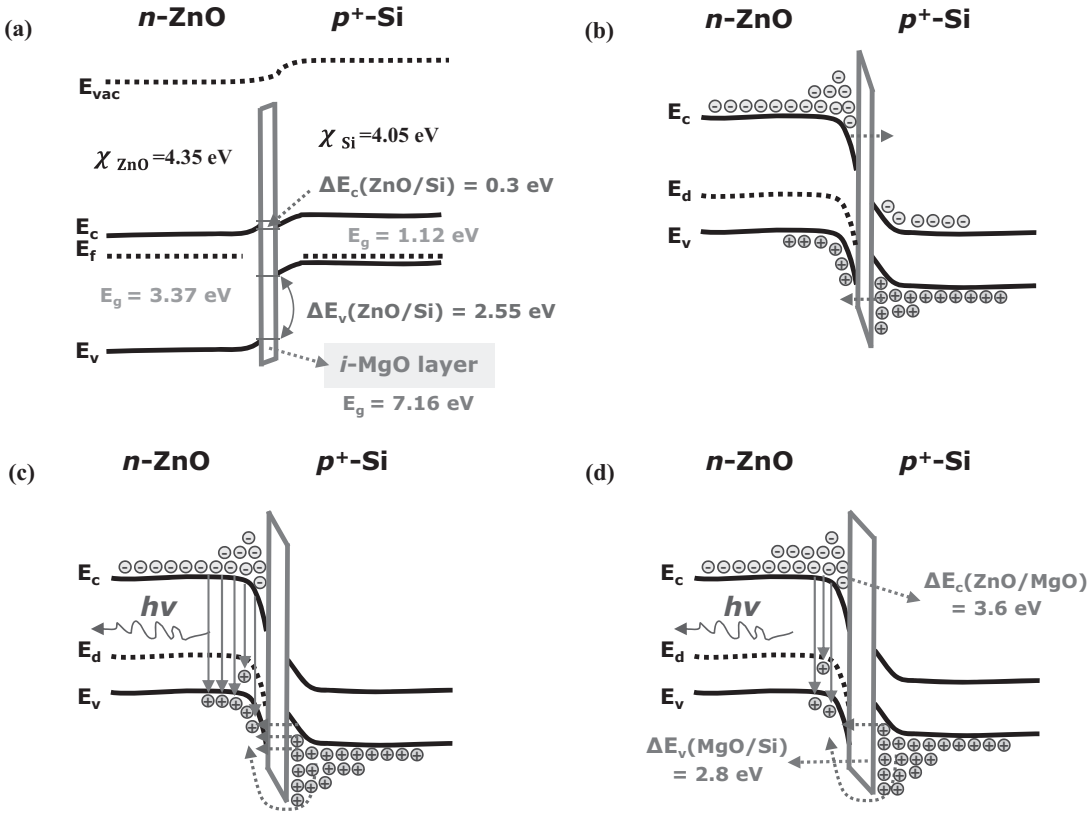

Figure 4. Energy band diagrams of the *n*-ZnO nanowires/*i*-MgO/p^+-Si heterostructures: (a) equilibrium state, (b) ultrathin MgO (sample 2), (c) thin MgO (sample 3), and (d) thick MgO (sample 4).

from Si to ZnO can also be expected, but the tunneling contribution is significantly reduced with increasing MgO thickness. As shown in Figures 2d and 4d, thicker *i*-MgO layers have reduced forward current levels due to suppression of the tunneling current. Consequently, it leads to a decrease in the EL intensity of the UV region, as shown in Fig. 3b. Therefore, the main mechanism for pure UV emission is due to the combination of the electron accumulation in the ZnO with high crystallinity by asymmetric band offset from insulating MgO and appropriate hole tunneling using thin *i*-MgO layers. Additionally, deep level emission (DLE) peaks in the EL emission are attributed to the recombination dropped from the conduction band of ZnO nanowires layer into deep level state,[27] and this contribution is relatively weak in sample 3.

Conclusions

ZnO nanowire based heterostructure LEDs have been fabricated by employing an insulating MgO dielectric layer as a carrier control layer and a ITO coated polymer sheet as an electrode on the top of the nanowires. We utilized the MOCVD for the growth of the ZnO nanowire and MgO layers, and controlled the thickness of MgO layers for searching the optimized UV LED structure. Consequently, the heterostructure LED with 4 nm MgO layer exhibited excellent UV EL emission. It was attributed that the *i*-MgO layer confined the electrons at the ZnO/MgO interfaces, and the relative small VBO and thin MgO induced selectively the hole injection from *p*-Si to ZnO, resulting in the effective radiative recombination in the ZnO region. Under forward bias, a sharp UV EL emission (around 380 nm) at room temperature was observed from the *n*-ZnO nanowires layer, together with weak visible emissions. For thick *i*-MgO thickness, the UV emission intensity became weak under the same driving voltage, and the threshold voltage and series resistance in the *I*-*V* curves were also increased. Such *n*-ZnO/*i*-MgO/*p*-Si heterojunction LEDs showed EL and PL emissions centered at similar positions due to nearly stress free ZnO nanowires.

Acknowledgments

This work was financially supported by the Grant Nos. 2011-0009494 and 2011-0001650 through the National Research Foundation of Korea funded by the Ministry of Education, Science and Technology (MEST).

References

1. M. H. Huang, S. Mao, H. Feick, H. Q. Yan, Y. Y. Wu, H. Kind, E. Weber, R. Russo, and P. D. Yang, *Science*, **292**, 1897 (2001).
2. D. C. Kim, B. O. Jung, J. H. Lee, H. K. Cho, and J. Y. Lee, *Nanotechnology*, **22**, 265506 (2011).
3. M. Law, L. E. Greene, J. C. Johnson, R. Saykally, and P. D. Yang, *Nat. Mater.*, **4**, 455 (2005).
4. D. C. Kim, W. S. Han, H. K. Cho, B. H. Kong, and H. S. Kim, *Appl. Phys. Lett.*, **91**, 231901 (2007).
5. D. C. Kim, S. K. Mohanta, and H. K. Cho, *Cryst. Growth. Des.*, **9**, 4725 (2009).
6. X. Bai, P. Gao, Z. L. Wang, and E. Wang, *Appl. Phys. Lett.*, **82**, 4806 (2003).
7. S. K. Mohanta, D. C. Kim, X. H. Zhang, C. B. Soh, A. M. Yong, H. K. Cho, and S. Tripathy, *J. Cryst. Growth*, **310**, 5312 (2008).
8. J. Y. Lao, J. Y. Huang, D. Z. Wang, Z. F. Ren, D. Steeves, B. Kimball, and W. Porter, *Appl. Phys. A: Mater. Sci. Process.*, **78**, 539 (2004).
9. D. C. Kim, W. S. Han, B. H. Kong, H. K. Cho, and C. H. Hong, *Physica B*, **401**, 386 (2007).
10. N. Bano, I. Hussain, O. Nur, M. Willander, P. Klason, and A. Henry, *Semicond. Sci. Technol.*, **24**, 125015 (2009).
11. H. Long, G. Fang, H. Huang, X. Mo, W. Xia, B. Dong, X. Meng, and X. Zhao, *Appl. Phys. Lett.*, **95**, 013509 (2009).
12. Y. I. Alivov, E. V. Kalinina, A. E. Cherenkov, D. C. Look, B. M. Ataev, A. K. Omaev, M. V. Chukichev, and D. M. Bagnall, *Appl. Phys. Lett.*, **83**, 4719 (2003).
13. C. Y. Huang, Y. J. Yang, J. Y. Chen, C. H. Wang, Y. F. Chen, L. S. Hong, C. S. Liu, and C. Y. Wu, *Appl. Phys. Lett.*, **97**, 013503 (2010).
14. D. C. Kim, J. H. Lee, S. K. Mohanta, H. K. Cho, H. Kim, and J. Y. Lee, *CrystEngComm*, **13**, 813 (2011).

15. P. Vinod, *J. Mater. Sci.: Mater. Electron.*, **21**, 730 (2010).
16. Y. P. Hsieh, H. Y. Chen, M. Z. Lin, S. C. Shiu, M. Hofmann, M. Y. Chern, X. Jia, Y. J. Yang, H. J. Chang, and H. M. Huang, *Nano Lett.*, **9**, 1839 (2009).
17. K. R. Jeon, C. Y. Park, and S. C. Shin, *Cryst. Growth. Des.*, **10**, 1346 (2010).
18. H. K. Yu and J.-L. Lee, *Cryst. Growth. Des.*, **10**, 5200 (2010).
19. W. S. Han, Y. Y. Kim, B. H. Kong, H. K. Cho, J. Y. Moon, and H. S. Lee, *Jpn. J. Appl. Phys.*, **48**, 08HK03 (2009).
20. J. Kim and Y. Yamamoto, *Phys. Rev. B.*, **55**, 9949 (1997).
21. S. W. Lee, H. D. Cho, G. Panin, and T. Won Kang, *Appl. Phys. Lett.*, **98**, 093110 (2011).
22. C. H. Ahn, Y. Y. Kim, D. C. Kim, S. K. Mohanta, and H. K. Cho, *J. Appl. Phys.*, **105**, 013502 (2009).
23. J. A. Aranovich, D. Golmayo, A. L. Fahrenbruch, and R. H. Bube, *J. Appl. Phys.*, **51**, 4260 (1980).
24. S. M. Sze and K. K. Ng, *Physics of semiconductor devices*, Wiley (2007).
25. J. Yamashita, *Phys. Rev.*, **111**, 733 (1958).
26. H. Zhu, C. Shan, L. Wang, Y. Yang, J. Zhang, B. Yao, D. Shen, and X. Fan, *Appl. Phys. Lett.*, **96**, 041110 (2010).
27. Z. Shi, L. Zhao, X. Xia, W. Zhao, H. Wang, J. Wang, X. Dong, B. Zhang, and G. Du, *J. Lumin.*, **131**, 1645 (2011).